





Experimental and Computational Studies of Nitric Acid Treated Natural Sargassum Algae for Efficient Removal of Crystal-Violet Dye

Hussein S. Mohamed¹ , Zeinab S. Hamza¹, Wael Z. Tawfik², Nada A. Mohammed¹, H. R. Abd El-Mageed³, N. K. Soliman⁴, Amany H. El-Zairy¹, and Momtaz Y. Hegab^{5,6} 

¹Chemistry of medicinal and aromatic plants department, Research Institute of Medicinal and Aromatic plants (RIMAB), Beni-Suef University, Beni-Suef 62511, Egypt

²Department of Physics, Faculty of Science, Beni-Suef University, Beni-Suef 62511, Egypt

³Micro-Analysis and Environmental Research and Community Services Center, Faculty of Science, Beni-Suef University, Beni-Suef City, Egypt

⁴Basic Science Department, Nahda University, Beni-Suef University, Beni-Suef 62511, Egypt

⁵Department of Botany, Faculty of Science, Beni-Suef University, Beni-Suef 62511, Egypt

⁶Research Institute of Medicinal and Aromatic plants (RIMAB), Beni-Suef University, Beni-Suef 62511, Egypt

Abstract: In this work, crystal-violet (CV) dye was removed using a chemical carbonization process to create carbonized sargassum algae (CSA), which poses less environmental danger. The produced CSA is examined using a scanning electron microscope and a Fourier-Transform Infrared spectrometer. The following parameters were measured: pH, contact duration, temperature, adsorbent concentration, and starting CV dye concentration. The highest removal % was recorded as 91.17%. at pH 7, 3 hours, 25 °C, 0.01 g of adsorbent dosage, and 100 mg/L initial dye concentration. The kinetic testing indicated that pseudo-second-order was the most effective kinetic model for CV adsorption. According to the isotherms for the adsorption of CV dye, the Langmuir constant (K) was used to measure thermodynamic properties like free enthalpy (H), entropy (S), and energy (G). The Freundlich model, followed by Temkin models, best described the data. The earlier research is supported by computational studies like molecular dynamics (MD) simulation and Monte Carlo (MC) simulation.

Keywords: Sargassum, crystal violet, adsorption, kinetics, MD simulation.

Submitted: April 26, 2023. **Accepted:** July 13, 2023.

Cite this: Mohamed HS, Hamza ZS, Tawfik WZ, Mohammed NA, Abd El-Mageed HR, Soliman NK, El-Zairy HA, Hegab MY. Experimentally and Computational Studies of Nitric Acid Treated Natural Sargassum Algae for Efficient Removal of Crystal-Violet Dye. JOTCSA.2023;10(4):903-18.

DOI: <https://doi.org/10.18596/jotcsa.1287989>.

***Corresponding author. E-mail:** h_gendy_2010@yahoo.com, Phone: +201000800296.

1. INTRODUCTION

Life and survival depend on access to enough clean water. Dyes, phenols, detergents, pesticides, heavy metals, and other air pollutants that are found in water sources come from domestic, industrial, and agricultural pollution sources.(1, 2). Today, a wide range of companies, including those in the paper,

printing, pharmaceutical, and cosmetics sectors, employ dyes in essential ways to color their goods. Over 20% of the coloring is discharged into the aquatic environment during the coloring process.(3). the crystal violet dye's chemical composition $C_{25}N_3H_{30}Cl$ is one of these cationic dyes, and it is employed for coating, coloring, and dyeing among other things. Environmental contaminants like CV,

although having a wide range of applications, have been referred to as biohazard dyes and refractory dye molecules that stay in the environment for a long time and have a harmful influence on the ecosystem. (4-6). Industries related to dyes use vast volumes of dyes, which are particularly harmful to aquatic life and even relatively harmless in the aquatic environment (7, 8). The ecological equilibrium of the water and aquatic life is disturbed by dyes because they prevent light from flowing through, absorb it, and reflect it back, triggering a process that prevents photosynthesis (9-11). Effects from the dye release may be felt by those who use water for drinking, washing, bathing, and other activities. Certain teeth can result in allergies, skin problems, and mutagenesis consequences in living organisms(12-15). Numerous methods, including oxidation, clotting, photo-degradation, precipitation, membrane filtration, electric flotations, and ion exchange, have been created as a result of the threat that dyes bring to marine life(16-18) and other physical/chemical techniques have been employed. It also talks about oxidation. However, due to their high prices and various disadvantages, small and medium-sized firms are unable to employ these approaches to manage bulk. The adsorption technique seems to be the most efficient way to treat wastewater due to its simplicity, low cost, reduced energy consumption, ease of operation, negligible effects of highly toxic materials, and the primary quality of emission handled for well-engineered sorption systems.(19). One of the wastewater chemical contaminants unit activities is adsorption (6, 20-27). Activated carbon (AC) is the most widely used adsorbent for treating wastewater or removing contaminants from wastewater(25, 28-33). Flax fiber, sugarcane bagasse, and pine tree wood are just a few of the raw ingredients utilized to create AC(15, 21, 23, 34, 35). Without any surface modification, activated carbon has a very poor adsorption capacity due to its small specific area. In some cases, it becomes crucial to treat the activated carbon to increase its capacity for bonds, which in turn raises its capacity for adsorption. Numerous methods, including physical, chemical, and biological ones, are employed for the surface treatment of activated carbon(35). Treatment of activated carbon, also known as surfactant modification, is essential. Activated carbon is treated with surfactants to create a strong bond with water, increasing the dispersion and solubility of AC in water(6). The period of adsorption depends on how well the thermodynamic and adsorbent mass transfer work (36-38). Marine algae known as seabed have large metal binding capabilities because they feature polysaccharides, proteins, or lipids on the surface of the cell wall that contain functional groups like amino, hydroxyl, carboxy, and sulphate that can serve as binding sites for metals (39-41). The thallus structures that resemble sheets and have a thickness of two cells are created by a

broad region of uniform and active cells in sargassum(23, 42). In this study, experimental factors for the adsorption process, such as mass, pH, temperature, duration of contact, and concentration, were looked at. The Freundlich and Langmuir adsorption isotherm equations were fitted to the equilibrium biosorption data. In order to understand the nature of the system, measurements of thermodynamic parameters were also made. Monte Carlo (MC) simulation and molecular dynamic (MD) simulation studies were carried out to examine the adsorption of crystal violet dye on the carbonized sargassum algae and to determine the desorption sites of crystal violet dye on the surface.

2. EXPERIMENTAL METHOD

2.1. Collection of Sargassum

Ras Sudr Was Used To Collect Sargassum Algae. Ras Sudr Is Located On The Red Sea Shore Of The Gulf Of Suez At A Longitude Of 32° 43' East And A Latitude Of 29° 35' North. It Is Included In The South Sinai Governorate. Ras Sudr Is Located On The Sinai Peninsula's Western Side, Around 200 Kilometers From Cairo And 60 Kilometers From The Ahmed Hamdi Tunnel Crossing In Suez. Ayn El Sokhna, A Resort On The Opposite Red Shore, Is Also Literally Across The Street. Ras Sudr Has A Coastline Of 95 Kilometers.

2.2. Preparation of Carbonized Sargassum Algae

Sargassum was cleaned with water to remove any remaining soil before being dried for 48 hours at room temperature (25 °C). Sargassum was then crushed into little pieces. After soaking in nitric acid (Sigma, 99.99%) for 24 hours, it was dried for another 24 hours at 100 °C. The solid mass was then immersed in filtered water for 24 hours before being dried for 6 hours at 40 degrees Celsius. It was then soaked in sulfuric acid for 6 hours before being dried for 12 hours at 100 °C. The completed product was carbonized for 3 hours at 500 °C.

2.3. Characterization

To characterize the CSA derived from sargassum algae, various approaches were applied. FTIR was utilized to examine the chemical structure. An X-ray diffractometer (XRD; type Ultima-IV; Rigaku, Japan) was used to measure CSA. At room temperature, FTIR spectrometer (VERTEX 70 FT-IR) spectra were recorded on ATR discs in the wave number range 4000-600 cm⁻¹. A scanning electron microscope (SEM) model JSM-6510LA was used to characterize surface morphology. Samples were made by placing a tiny film on a carbon tube on a stub covered with a thin layer of gold.

2.4. Adsorption Experiments

To characterize the CSA derived from sargassum algae, various approaches were applied. FTIR was utilized to examine the chemical structure. An X-ray diffractometer (XRD; type Ultima-IV; Rigaku, A set of dye solutions of varied concentrations is created. A series of adsorption tests were performed on CSA

adsorbent under varied reaction circumstances, including beginning dye concentration (10, 25, 50, and 100 mg/L), temperature ranging from 25 to 60 °C, CSA dosage of 0.01-0.04 g per 50 mL of solution, and solution initial pH (2-10). The contacting time in both tests was 180 minutes, and the solution volume was 50 mL. The shifts in the tested CV dye concentration were determined using a UV-vis spectrophotometer and its characteristic absorption peaks (max= 592 nm). The first set of experiments were conducted with the adsorbent dosage remaining constant at 0.01 g per 50 mL of solution, the pH remaining constant at 7, the temperature remaining constant at 25 °C, and the dye concentration varying between 10, 25, 50, and 100 mg/L. The purpose of this experiment was to determine the effect of starting dye concentration on the percentage of CV removal over CSA adsorbents. In the second series, the dye starting concentration remained constant at 100 mg/L, the pH was set to 7, the temperature was set to 25°C, and the adsorbent dosage was varied from 0.01 to 0.04 g per 50 ml of solution. The purpose of this test was to determine the influence of adsorbent dosage on the percentage of CV dye removal over CSA adsorbents. The third series of studies involved adjusting the temperature from 25 °C to 60 °C while keeping the dye starting concentration at 100 mg/L, pH at 7, and adsorbent dosage at 0.01 g per 50 mL of solution constant. The purpose of this experiment was to determine the effect of temperature on the percentage of CV removed by CSA adsorbents. The third set of trials entailed adjusting the solution's starting pH from 2 to 10, while keeping the dye initial concentration constant at 100 mg/L, at a temperature of 25 °C, and with an adsorbent dosage of 0.01 g per 50 mL of solution. The purpose of this experiment was to examine the effect of pH on the percentage of CV dye removal over CSA adsorbents. By adding dilute HCl and NaOH dropwise, the pH was adjusted to the right amounts. Equations (1) through (3) can be used to calculate the amount of dye extracted by sargassum adsorbents at equilibrium (q_e (mg/g)), the amount of dye removed by sargassum adsorbents at any time (q_t), and the dye removal percentage. (43, 44).

$$q_e = (C_0 - C_e) \frac{V}{m} \tag{1}$$

$$q_t = (C_0 - C_t) \frac{V}{m} \tag{2}$$

$$\text{Dye removal \%} = \frac{(C_{0c} - C_t)}{C} \times 100 \tag{3}$$

where C_0 denotes the initial dye concentration in mg/L, C_t denotes the dye concentration in mg/L over time t , C_e denotes the dye concentration in mg/L at equilibration, and m denotes the CAB V is the solution volume in milliliters, and m is the mass in milligrams.

2.5. Kinetic Studies

The kinetics of CV adsorption studies on CSA were carried out using 0.01 g of adsorbent at CV concentrations of 10, 25, 50, and 100 mg/L, adsorption periods ranging from 10 to 180 minutes, temperatures of 25 °C, and pH of 7. Adsorption kinetics were evaluated using models such as pseudo first order, pseudo second order, Elovich, and intra-particle adsorption.

2.5.1. Pseudo-first-order model

The Lagergren's pseudo-first-order equation (45)

$$\log(q_e - q_t) = \log(q_e) - K_1 t / 2.303 \tag{4}$$

Where q_e and q_t are the amounts of dye absorbed on the CSA at equilibrium and the amount of dye absorbed at any time t , respectively. K_1 the constant rate of the pseudo first order.

2.5.2. Pseudo-second-order Model

Pseudo-second-order model is represented by following equation formulated by (46)

$$\frac{t}{q_t} = \frac{1}{K_2} q_e^2 + \frac{t}{q_e} \tag{5}$$

where K_2 is the constant rate of the pseudo second order. The parameters of kinetic model with R_2 are compared in the Table 2. R^2 values show that the pseudo second order is better than the other.

2.5.3. Intraparticle diffusion model

It is represented by using the following equation(47)

$$q_t = K_{int} t^{1/2} + C \tag{6}$$

where K_{int} is the intraparticle diffusion constant and C is the intercept.

2.5.4. Elovich kinetic model

The equation of it has the following form(48)

$$\frac{q}{q_e} = \frac{1}{\beta q_e} \ln(\alpha \beta) + \frac{1}{\beta q_e} \ln t \tag{7}$$

where, α is the initial adsorption rate and β is the relationship between the degree of surface coverage and the activation energy involved in the chemisorption.

2.6. Adsorption isotherm

It depicts the distribution of the solute in two phases (liquid and adsorbed). The Langmuir, Freundlich, and Temkin isotherms were used to research adsorption isotherms.(49)

2.6.1. The Langmuir isotherm

It is used, for homogeneous adsorption, and its linearized form can be defined by the equation below (50).

$$\frac{C_e}{q_e} = \frac{1}{K_a Q_0} + \frac{C_e}{Q_0} \quad (8)$$

where q_e (mg/g) and C_e (mg/L) are the amounts of dye adsorbed per unit mass of adsorbent and unadsorbed dye concentration in the solution, Q_0 is the maximum amount of dye adsorbed per unit mass of adsorbent on the entire monolayer surface, and K_a is a constant related to the affinity of the binding sites.

2.6.2. Freundlich isotherm model

This is used for heterogeneous surface at different temperatures. It has the following form (51):

$$\log q_e = \log k_f + \log \frac{C_e}{n} \quad (9)$$

where K_f is the Freundlich constant, and $1/n$ is the heterogeneity factor.

2.6.3. Temkin isotherm

It has the following form:

$$Q_e = BT \ln KT + BT \ln C_e \quad (10)$$

where, $B T$ is a temperature dependent constant related to the heat of adsorption $K T$ and is the equilibrium constant. The degree of favorability of the Langmuir isotherms for the equilibrium data could be predicted from the value of (R_L) the dimensionless separation factor constant that can be determined from Equation 11 (52).

$$R_L = \frac{1}{1 + K_L C_{max}} \quad (11)$$

where C_{max} represents the maximum initial DR concentration.

2.7. Thermodynamic Parameters

Thermodynamic parameters such as standard free energy, enthalpy, and entropy are used (53). The following calculations were used to assess the effect of heat on the adsorption period at various dye concentrations.

$$K_{id} = \frac{q_e}{C_e} \quad (12)$$

$$\Delta G^0 = -RT \ln K_{id} \quad (13)$$

$$\ln K_{id} = \frac{\Delta S^0}{R} - \frac{\Delta H^0}{RT} \quad (14)$$

Where $K = b$ is the adsorption equilibrium constant, R is the gas constant (8.314 J/K mol), T is the absolute temperature, ΔH^0 enthalpy, ΔS^0 entropy ΔS and ΔG^0 free energy.

2.8. Computational Details

2.8.1. Monte Carlo (MC) simulation

MC simulation was conducted in this work to study the adsorption of crystal violet dye on the carbonized sargassum algae and to find the desorption sites of crystal violet dye on the carbonized sargassum algae surface. MC simulation was carried out by Adsorption Locator module as shown in this study(54, 55) using The COMPASS force field (Condensed-phase Optimized Molecular Potentials for Atomistic Simulation Studies) as a force field and use current in the charges section. The basic principles of MC simulation used in this work have been described by Frenkel and Smit (56).

2.8.2. Molecular dynamics (MD) simulation

In the MD simulations, the electrostatic and van der Waals terms were treated with Ewald and group-based methods, respectively. The MD was simulated under NPT ensemble for 1 ns, followed by isothermal-isobaric (NPT) conditions at 1 atm and 300 K for 4 ns, with time step of 1 fs. The temperature and pressure were controlled by Nose thermostat and Berendsen barostat, respectively. The velocity Verlet algorithm was used in the integration of the equations of motion (57). The theoretical background of MD simulation is done according to this study (55).

3. RESULTS AND DISCUSSION

3.1. Analysis of Carbonized Sargassum Algae

FTIR and SEM were performed to analyze the chemical composition.

3.1.1. FTIR spectrum

After loading the crude powder of Nitric acid-treated natural sargassum algae into the FT-IR, the primary functional group of the components was separated based on the peak ratio. The functional groups of bioactive components are denoted by the peak values of the FTIR spectrum (Figure 1 and Table 1). In the FT-IR spectrum of Nitric acid-treated natural sargassum algae, peaks at 3722, 3375, 2954, 2412, 2470, 2353, 2206, 1494, 1363, 1222, 1078, 871, 732, 628 and 559 cm^{-1} were discovered. The stretching vibrations of CH, C-C, and C-O in solid band, as well as C-O stretch mode in signals at 3375-559 cm^{-1} , mirrored the axial position stretching vibrations of OH. According to research, the absorption bands between 1100 and 1000 cm^{-1} are crucial for carbohydrates and polysaccharides, pointing to a variety of mechanisms such as C-H deformation, C-O or C-C stretching (58, 59). The toxic interaction sites of algae's carboxyl, amino acid, and hydroxyl groups were investigated using FT-IR spectra of seaweed extracts (60, 61). A new survey found the bands in diverse materials at significantly different frequencies, with peaks of 1222 and 1078 cm^{-1} . Carbohydrates were found to be the most effective absorbers between 1200 and 1000 cm^{-1} in those samples (62). In nucleic acids, as in a variety of other molecules, identical absorption bands in the same spectral area of similar functional groups were found.

3.1.2. SEM analysis

Scanning electron micrographs (SEM) of carbonized sargassum algae at low and high magnification are shown in Figure 2. When the sargassum algae was treated with nitric acid at high temperatures, it disintegrated dramatically and the surface of the sample began to shrink, possibly due to nitric acid's partial loss of hemicellulose. Furthermore, the high temperature may have caused the cellulose fibers to be liberated from their initial clusters.

3.2. Optimization of Parameters

3.2.1. Dye's initial concentration

Figure 3 shows how dye starting concentrations and contact time affect removal percentages and adsorption capacities when CSA is used as an adsorbent. Figure 3 demonstrates that with an initial concentration of 100 mg/L, the adsorption percentage for diffuse CV dye achieved 91.17 %.

Table 1: FTIR peak value of Nitric acid-treated natural sargassum algae.

S. No.	Peak Value	Spectroscopic Assignments	Functional Groups
1.	2375	O-H stretch, H-bonded	Alcohols, Phenols
2.	2353	O-H stretch	Carboxylic acids
3.	2954	-C≡C- stretch	Alkynes
4.	1631.080	C-C stretch (in-ring)	Aromatics
5.	1363,1494,1222	C-H bend	Alkanes
6.	1078	C-O stretch	Alcohols, Carboxylic acids, Esters, Ethers
7.	871,732,628,559	-C≡C-H: C-H bend	Alkynes

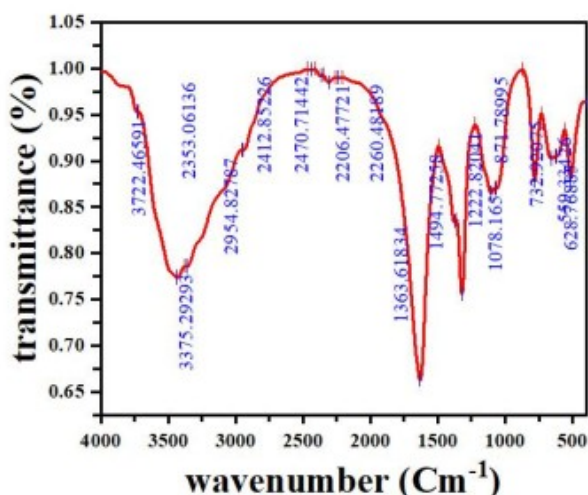


Figure 1: FT-IR of the crude powder of Nitric acid-treated natural sargassum algae.

The presence of a large number of free adsorption sites on the adsorbent surface can explain the quick adsorption rate observed during the primary stage of adsorption processes. The adsorbed dye molecules fill the exposed areas over time, generating in a repulsive force between the adsorbate scatter CV dye molecules on the CSA surface and those in the bulk liquid form. When it comes to CSA, the percentage of diffuse CV dye removal normally increases as the dye level

increases. Figure 3 shows that when the original diffuse CV dye concentration increases, so does the sum of adsorbed dyes. This could be attributable to an increase in concentration gradient as diffuse CV dye starting concentration increases. As a result, the driving power increases and is required to overcome the resistance to mass transfer between adsorbate and adsorbent (43, 63).

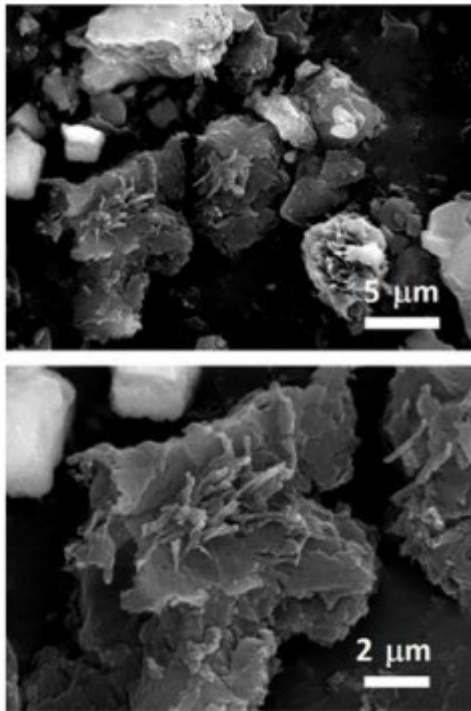


Figure 2: SEM images of carbonized sargassum algae.

3.2.2. Effect of adsorbent weight mass

We researched the effect of CSA adsorbent doses on the removal percent of disperse crystal violet dye to establish the optimal adsorbent weight that gives the highest performance in order to calculate the wastewater treatment cost per unit of disperse crystal violet dye using CSA adsorbent. Figure 4(a) depicts the influence of CSA weight on the scatter crystal violet dye removal percent. The dye removal % increases as the CSA weight increases from 0.01 to 0.04 g per 50 mL of disperse crystal violet dye solution at an initial concentration of 100 mg/L at 25°C and pH 7. The dye removal percentage improved to 91.17 %, which may be attributed to increased surface area and the number of surface-active sites accessible for adsorption as adsorbent dosage was raised. (64). The best adsorption at dose 0.01 g.

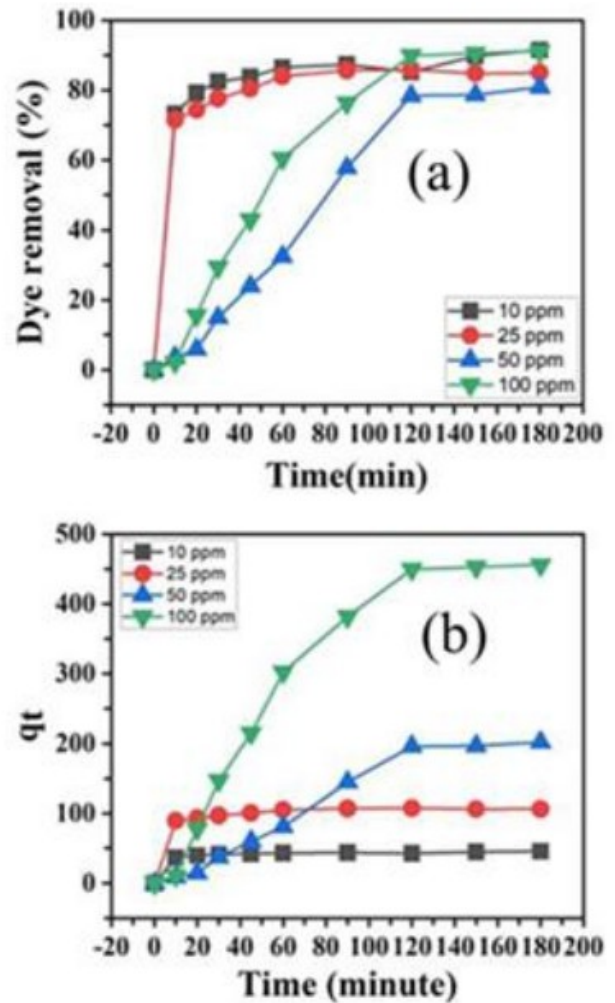


Figure 3: Effect of CV dye concentrations and contact time on (a) the removal % of dye adsorbed and (b) the amount of dye adsorbed at 25 °C and pH 7 by 10 mg of adsorbent.

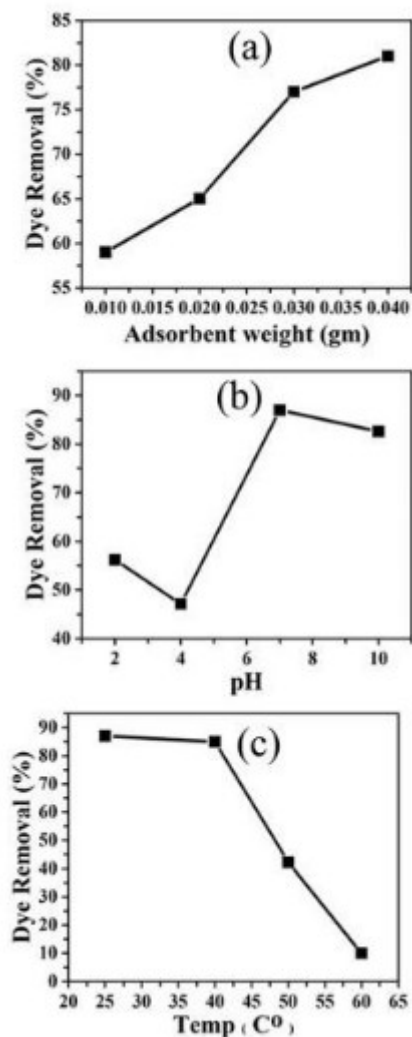


Figure 4: Effect of adsorption conditions on the removal % of CV dye by carbonized sargassum algae. Where (a) represent the effect of adsorbent weight. (b) represent the effect of Initial pH of the solution. (c) represent the effect of adsorption temperature.

3.2.3. Initial pH of the solution

The pH regulates the amount of electrostatic charge on the sorbent and sorbate. Because of their effect on ionization/dissociation of the sorbent molecules and their effect on the adsorbent surface, pH of the solution plays an important role in adsorption power (65). The effect of the initial pH values of the aqueous dye solutions on the removal percent of diffuse CV dye using CSA sorbent is seen in Figure 4(b). Because of the high concentration of hydrogen (H+) ions and the protonation of the adsorbent base, the elimination percentage generally increases as the pH value increases from 2 to 7 (66). The dye anions are drawn strongly to the positively charged adsorbent surface (67, 68). In other words, as the pH of the CSA increases, the surface becomes negatively charged, causing the polarization of the electric double layers to reverse. As a result, as seen in Figure 2, the adsorption percentage of diffuse CV

dye decreases (b)(69). The maximum amount of adsorbed at pH 7.

3.2.4. Effect of adsorption temperature

The temperature effect on the adsorption of industrial disperse CV dye over CSA was studied at four different reaction temperatures (25 °C, 40 °C, 50 °C, and 60 °C), and the results are shown in Figure 4. (c). The dye removal percentage for CSA falls significantly as the temperature rises from 25 °C to 60 °C. The negative value H (see section (3-5) thermodynamic study) confirms that the adsorption of disperse CV dye onto CSA was an exothermic phase. The higher temperature stability of CSA adsorbent demonstrated that temperature had little effect on the adsorption forces between the adsorbent (CSA active sites) and adsorbate (disperse CV dye molecules)(70). The higher attraction between adsorbate active sites and ions of dye molecules resulted in the beneficial adsorption of CV at a relatively low temperature. The percentage of diffuse crystal violet dye removal decreased as the temperature increased from 25°C to 60°C. 25°C is the optimal temperature for diffuse crystal violet dye adsorption over CSA adsorbent.

3.3. Adsorption Isotherm

The statistical significance of R² (the correlation coefficient) for the linear plots of Ce/qe versus Ce, log qe against log Ce and qe against Ln Ce was the criteria by which the data fitting to the Langmuir, Freundlich, and Temkin isotherms was checked (Figure 5). The estimated values of Q₀, K_L, K_F, and 1/n, K_T, and B, and R² were determined from the linear plots and reported in Table 2. CV adsorption on CSA adsorbent does not follow the Temkin and Langmuir isotherm models (Table 2). The Freundlich isotherm model has the maximum R² value; the adsorption mechanism almost follows the Freundlich isothermal model. As a result, the dye is eliminated at the active sites of the CSA adsorbent on a single surface plate, and the adsorbed CV molecules do not react with one another. The R² value determined by the Langmuir isotherms at 25 °C was 0.2092. The value of R_L is 1, meaning that the adsorption of CV in the study case is beneficial (2). The overall adsorption potential of CSA according to the Langmuir adsorption isotherm is 666 mg/g.

3.4. Adsorption Kinetics

To study the most suitable adsorption kinetics model, the adsorption process of CV on CSA under various initial dye concentrations was followed. The first-order, second order, intraparticle diffusion and Elovich kinetics linear graphs were represented by plotting ln (qe - qt) versus t, versus t, against and qt versus ln t, respectively, as shown in Figure 6(a-d), in order. The adsorption kinetics parameters k₁, k₂, k₃, q_e, I, β, and α of the evaluation model in addition to R² were calculated from the linear graph and depicted in Table 3. The linear fit and regression coefficient values (Table 3) for all the investigated kinetic models verified that the pseudo-second-order model adequately manages CV adsorption into CSA. Similarly, the values of q_e Exp. (measured q_e)

and q_e (calculated q_e) obtained from a pseudo-second order plot of all CV concentrations agree well (Table 3). The k_1 value (pseudo-secondary rate constant) and the CV concentration tested have an inverse relationship.

Table 2: Isotherm constants for CV adsorption onto 10 mg algae at 25 °C and pH 7.

Langmuir isotherm			
Q_o (mg/g)	K_L (L/mg)	R_L	R^2
666	0.71	0.013	0.2092
Freundlich isotherm			
1/n	K_F	R^2	
0.79	47.8	0.8368	
Temkin isotherm			
B (J/mol)	K_T (L/mol)	R^2	
118.5	1.35	0.5456	

Table 3: Parameters of the kinetic models for CV dye adsorption onto 0.01 g of algae at 25°C and pH 7.

First order kinetic model					
Dye concentration (ppm)	10	25	50	100	
K	0.007	0.010	0.011	0.015	
Q_e	2.9	4.2	12.1	18.1	
R^2	0.5458	0.7250	0.8908	0.9345	
q_{eexp}	45.7	106.2	202.1	455.8	
Second order kinetic model					
K	5.6×10^{-3}	3.5×10^{-3}	3.6×10^{-6}	1.2×10^{-6}	
q_e	45.8	108.3	-525	-1428	
R^2	0.9985	0.9996	0.2193	0.0347	
$q_e \text{ exp}$	45.7	106.2	202.1	455.8	
Elovich kinetic model					
β (g/mg)	0.366	0.152	0.012	0.005	
α (mg/min)	2.5×10^5	5.8×10^5	6	15.5	
R^2	0.9166	0.9112	0.9078	0.9769	
Intraparticle diffusion kinetic model					
K	2.3	5.6	18.6	42	
I	20.5	49.5	-43.5	-60.1	
R^2	0.5449	0.5410	0.9128	0.9391	

A straight line in the graph of q_t versus $t^{1/2}$ suggests that the intraparticle diffusion model is applicable. The slope and intercept of the plot can be used to calculate k_2 and I, and the results are seen in Table 3. The R^2 values (correlation coefficients) obtained from the model are relatively

small and unsatisfactory; additionally, the value of the intercept I is not zero, indicating that the intraparticle diffusion model may not be the only rate-controlling factor in deciding the kinetics of the adsorption mechanism. In comparison to the pseudo-first order, Elovich kinetics model, and intraparticle diffusion kinetic models, the pseudo-second-order kinetic model obtained a respectable correlation coefficient, indicating that CV adsorption on the CSA follows the pseudo-second-order rate model.

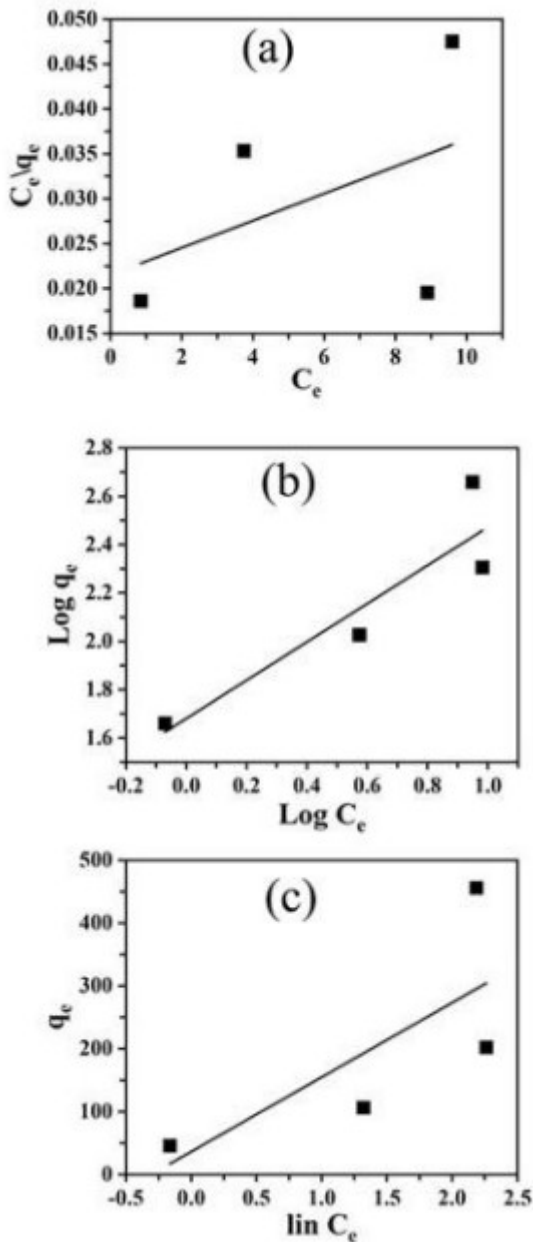


Figure 5: Plots of adsorption isotherm for the adsorption of CV dye by 10 mg of adsorbent at 25 °C and initial pH of the solution 7 where (a) represents Langmuir isotherms model, (b) Freundlich isotherms model and (c) Temkin isotherms model.

According to the data in Table 3, the pseudo-second-order paradigm is dominant. The pseudo-second-order adsorption process has two steps. The first step is an outward diffusion stage, in which CV molecules migrate from both sides of the solution to the CSA's outer surfaces. This is followed by a second stage in which CV molecules adsorb and adhere to the surfaces of CSA.

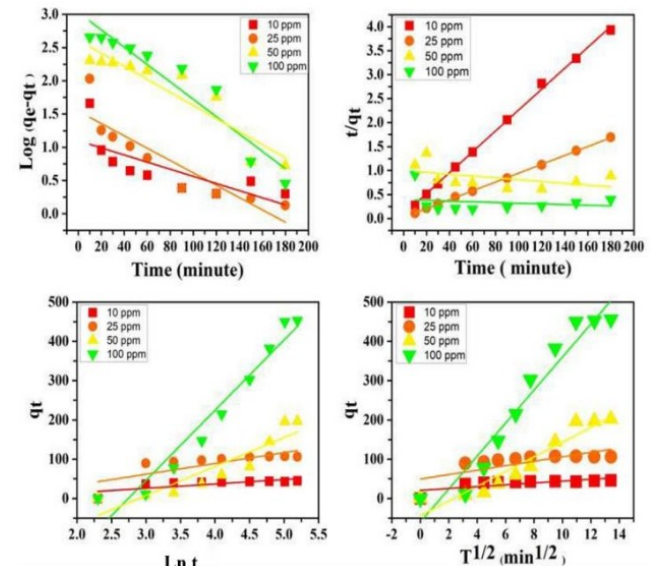


Figure 6: Sorption kinetics of CV dye at 25 °C and pH 7 by 10 mg of adsorbent where a) Represent Pseudo-first order, (b) Pseudo-second order, (c) Elovich kinetic model and (d) Intra-particle sorption.

3.5. Thermodynamic Study

Table 4 shows the thermodynamic parameters derived from CV adsorption on CSA adsorption thermodynamics. The negative ΔG value in Table 4 indicates that CV adsorption is a random operation. The change of the value of ΔG to a more correct value at higher temperatures shows that the adsorption mechanism is unfavorable at higher temperatures. The ΔG value ranges from -9.7 to 1.9 kJ/mol. These values are also within the physical adsorption range of ΔG (the physical adsorption range of ΔG is -20-0 kJ/ mol range), indicating that the adsorption mechanism on CSA is physical. The "n" value calculated by the Freundlich isotherm measurement model also confirms this finding, with a value greater than unity, representing a physical adsorption mechanism (71). Similarly, the RL value ranges between 0 and 1, indicating that CV adsorption is favorable under experimental conditions (72). The fact that the H value is negative indicates that the CV adsorption on CSA is an exothermic operation. The -ve value of S indicates a reduction in randomness at the solid/liquid interface as a result of CV adsorption on the surface of CSA (73).

3.6. MC Simulation

The lowest configuration obtained due to the adsorption of crystal violet dye on the carbonized sargassum algae surface in dry system (no solvent) is summarized in Figures 7. The aim of MC simulation is studying the adsorption of crystal violet dye on the carbonized sargassum algae and to find the desorption sites of crystal violet dye on the carbonized sargassum algae surface. The adsorption (ΔE_{ads}), interaction (E_{int}), and deformation (E_{def}) energies as well as substrate-adsorbate configurations (dE_{ads}/dNi), in which one of the adsorbate components has been removed, of crystal violet dye absorbed on the carbonized sargassum algae surface is displayed in Table 5. The crystal violet dye molecule has different hydrogen bond (HB) donor and acceptor sites. Thus, the oxygen atom of the cellulose carbonized sargassum algae has formed hydrogen bond with the hydrogen atom of crystal violet dye molecule with distance (1.70 Å) as shown in Figure 7. ΔE_{ads} crystal violet dye absorbed on the carbonized sargassum algae surface is negative which revealed that the adsorption of crystal violet dye absorbed on the carbonized sargassum algae surface is exothermic, energetically favorable and spontaneous, due to the existence of the intermolecular interactions. Also, it can be observed that the crystal violet dye absorbed on the carbonized sargassum algae surface following a parallel mode, which confirms the strong interactions between the crystal violet dye and the carbonized sargassum algae surface atoms. Analysis of the molecular structures of the crystal violet dye and the carbonized sargassum algae surface shows that the adsorption of the crystal violet dye onto the carbonized sargassum algae surface may be related to the contribution of the electrons of nitrogen, and oxygen (chemical adsorption). Furthermore, the Van Der Waals dispersion forces can also contribute to catch the crystal violet dye towards the carbonized sargassum algae (physical adsorption) which confirm the results obtained in the experimental part.

Table 4: Thermodynamic parameters for adsorption of CV dye onto algae.

Temperature (K)	ΔG (kJ/mol)	ΔH (kJ/mol)	ΔS (kJ/mol. K)
298	-9.7		
313	8.4		
323	-3.2	-108.9	-0.328
333	1.9		

Table 5: Adsorption energies (kcal/mol), Rigid adsorption energy, and Deformation energy, and substrate-adsorbate configurations (dE_{ads}/dNi) for the adsorption configuration of crystal violet dye on the algae doped activated carbon surface.

Adsorption energy	Rigid adsorption energy	Deformation energy	DR: dE_{ads}/dNi
-94.70	-34.39	-93.76	-651.21

3.7 MD Simulation

The MD simulation was used to investigate the influence of the presence of water solvent molecules on the adsorption of crystal violet dye on the carbonized sargassum algae surface, in which the configuration of crystal violet dye absorbed on the carbonized sargassum algae surface obtained from MC simulation was simulated in explicit water using MD. The ultimate simulation conformation of crystal violet dye carbonized sargassum algae was shown in Figure 8. The water molecules of aqueous solution moved freely to interact with the crystal violet dye and the carbonized sargassum algae during the simulations. MD snapshot at 5000 PS of the adsorption of crystal violet dye absorbed on the carbonized sargassum algae is shown in Figure 8. The crystal violet dye has different hydrogen bond (HB) donor and acceptor sites, and thus, it has formed several hydrogen bonds with the carbonized sargassum algae atoms. Also, the oxygen atoms of the carbonized sargassum algae were formed HBs with the hydroxyl hydrogen atoms of the crystal violet dye molecule. Figure 9 display that crystal violet dye molecule formed coordination bonds with carbonized sargassum algae atoms in water. In water system, intramolecular HBs between the functional groups of the crystal violet dye molecule, as well as HBs between crystal violet dye with water molecules, were observed. Thus, the MD simulation confirms that crystal violet dye is still interacts with the carbonized sargassum algae atoms even in presence of water molecules. Radial distribution function (RDF) was computed from the MD simulation to gain more insights into the stability of crystal violet dye- carbonized sargassum algae surface complex in water explicitly. This RDF can help us to understand the interaction between crystal violet molecule dye and the carbonized sargassum algae surface. RDF explained as the probability of locating particle "B" within the range ($r+dr$) of a particle A, and usually expressed as $g(r)$. It was used to investigate the interaction between crystal violet molecule dye and the carbonized sargassum algae surface, as well as describe the formation of hydrogen bonds with water. Figure 10 shows the RDF obtained due to the adsorption of crystal violet molecule on the carbonized sargassum algae surface atoms. As it can be seen from Figure 10 that the bonds RDF obtained due to the adsorption of crystal violet molecule on the carbonized sargassum algae surface atoms has a bond length= 2.3 Å. RDFs reveal that crystal violet

still interacts with the carbonized sargassum algae surface in the presence of water molecules.

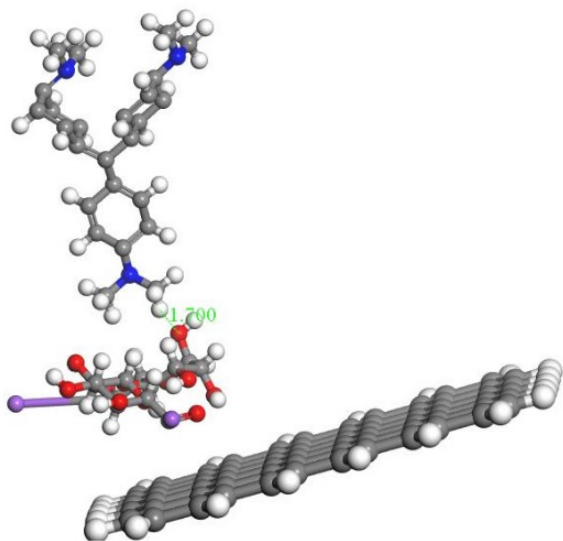


Figure 7: The adsorption configurations of the crystal violet dye onto the carbonized sargassum algal surface, obtained from MC simulation.

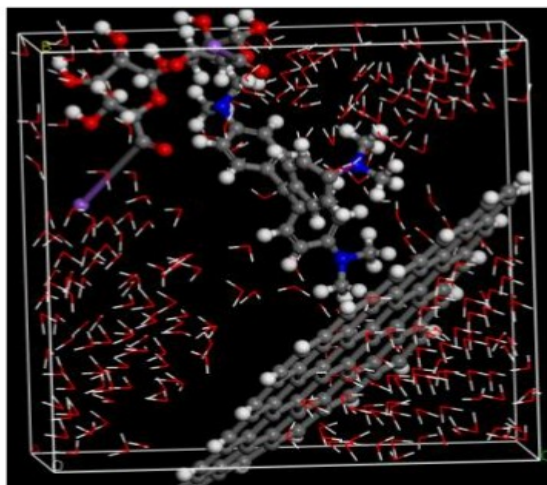


Figure 8: Simulation conformation of crystal violet dye absorbed on the carbonized sargassum algae.

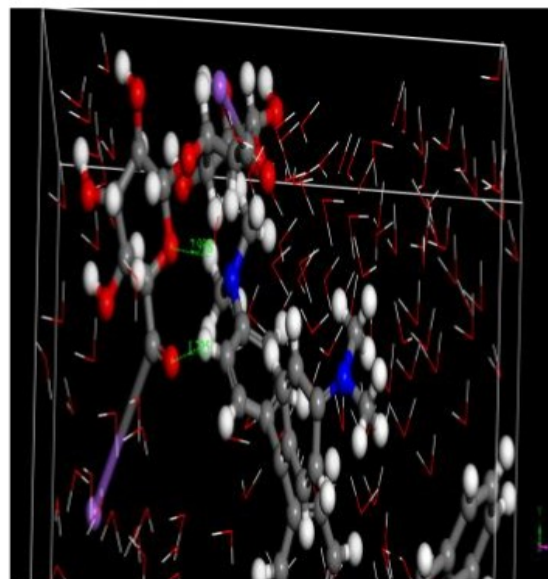


Figure 9: MD snapshots at 5000 ps of the adsorption of crystal violet dye on the carbonized sargassum algae surface, the bond length is in Ångströms.

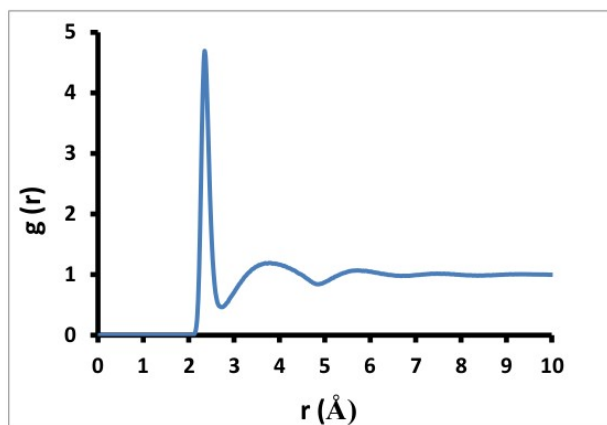


Figure 10: The RDFs for the adsorption of crystal violet dye on the carbonized sargassum algae surface atoms in the presence of water at 5 ns.

Table 6: Comparison among adsorption capacities of Crystal violet dye onto different adsorbents.

Seaweed Species	Sorption capacity (mg g ⁻¹)	Refs.
Activated carbons derived from male flowers of coconut tree	60.42	(74)
Kaolinite-supported nanoscale zero-valent iron	129	(75)
Merck activated carbon	67.09	(76)
Grapefruit peel	259.91	(77)
Zeolite from bottom ash	17.6	(78)
Raw <i>S. latifolium</i>	4.926	(41)
carbonized sargassum algae	666	This work

3.8. Comparison Between Our Study and Other Studies

Carbonized Sargassum seaweed (CSA) used in the study is a low cost adsorbent with high removal capacity (Table 6).

4. CONCLUSION

This paper looked into the adsorption of CV on an algae (Sargassum sp.) CSA preparation. The findings of this work support the notion that CSA is an effective low-cost adsorbent for extracting CV from aqueous solutions. CV adsorption is influenced by the initial dye concentration, contact time, adsorbent weight density, pH, and temperature. Maximum CV removal on CSA occurs when the starting dye concentration is 100 mg/L, the contact time is 3 hours, the adsorbent weight mass is 0.01 g, the pH is 7, and the temperature is 25°C (room temperature), the highest removal % was recorded as 91.17 % (666 mg/g). Freundlich's isothermal adsorption is depicted, and kinetics analysis results are correlated using a pseudo-second-order model. Monte Carlo (MC) and molecular dynamic (MD) simulation studies were performed to investigate the adsorption of crystal violet dye on the carbonized sargassum algae surface and to identify crystal violet dye desorption sites on the carbonized sargassum algae surface. The MC simulation reveals that the adsorption of Eads crystal violet dye on the carbonized sargassum algae surface is negative, indicating that the adsorption of crystal violet dye on the algae doped activated carbon surface is exothermic, energetically favorable, and spontaneous, owing to the presence of intermolecular interactions. The MD simulation reveals that even in the presence of water molecules, crystal violet dye interacts with the carbonized sargassum algae atoms. RDFs reveal that crystal violet still interacts with the carbonized sargassum algae surface in the presence of water molecules.

5. CONFLICT OF INTEREST

The authors declare no conflict of interest.

6. REFERENCES

- 1 Nemerow N. Liquid waste of industry: theories, practices and treatment. Addison-Wesley Publishing Company; 1971.
- 2 Nemerow NL. Liquid waste of industry. Theories, practices, and treatment. Addison-Wesley Publishing Company Inc, 8. 1971:590.
- 3 Al-Degs YS, El-Barghouthi MI, El-Sheikh AH, Walker GM. Effect of solution pH, ionic strength, and temperature on adsorption behavior of reactive dyes on activated carbon. Dyes and pigments. 2008;77(1):16-23. Available from: [<URL>](#).
- 4 Ju Y, Fang J, Liu X, Xu Z, Ren X, Sun C, et al. Photodegradation of crystal violet in TiO₂ suspensions using UV-vis irradiation from two microwave-powered electrodeless discharge lamps (EDL-2): Products, mechanism and feasibility. Journal of Hazardous Materials. 2011;185(2-3):1489-98. Available from: [<URL>](#).
- 5 Miyah Y, Lahrchi A, Idrissi M, Boujraf S, Taouda H, Zerrouq F. Assessment of adsorption kinetics for removal potential of Crystal Violet dye from aqueous solutions using Moroccan pyrophyllite. Journal of the Association of Arab Universities for Basic and Applied Sciences. 2017;23:20-8. Available from: [<URL>](#).
- 6 Goswami R, Dey AKJAS, Technology. Use of anionic surfactant-modified activated carbon for efficient adsorptive removal of crystal violet dye. 2022;2022. Available from: [<URL>](#).
- 7 Zare K, Sadegh H, Shahryari-Ghoshekandi R, Maazinejad B, Ali V, Tyagi I, et al. Enhanced removal of toxic Congo red dye using multi walled carbon nanotubes: kinetic, equilibrium studies and its comparison with other adsorbents. Journal of Molecular Liquids. 2015;212:266-71. Available from: [<URL>](#).
- 8 Sebeia N, Jabli M, Ghith A, Elghoul Y, Alminderej FM. Production of cellulose from Aegagropila Linnaei macro-algae: Chemical modification, characterization and application for the bio-sorption of cationic and anionic dyes from water. International journal of biological macromolecules. 2019;135:152-62. Available from: [<URL>](#).
- 9 Allen S, Mckay G, Porter JF. Adsorption isotherm models for basic dye adsorption by peat in single and binary component systems. Journal of colloid and interface science. 2004;280(2):322-33. Available from: [<URL>](#).
- 10 Sebeia N, Jabli M, Ghith A, El Ghoul Y, Alminderej FM. Populus tremula, Nerium oleander and Pergularia tomentosa seed fibers as sources of cellulose and lignin for the bio-sorption of methylene blue. International journal of biological macromolecules. 2019;121:655-65. Available from: [<URL>](#).
- 11 Jabli M. Synthesis, characterization, and assessment of cationic and anionic dye adsorption performance of functionalized silica immobilized chitosan bio-polymer. International journal of biological macromolecules. 2020;153:305-16. Available from: [<URL>](#).
- 12 Bhatnagar A, Jain A. A comparative adsorption study with different industrial wastes as adsorbents for the removal of cationic dyes from water. Journal of Colloid and Interface Science. 2005;281(1):49-55. Available from: [<URL>](#).
- 13 Jabli M, Gamha E, Sebeia N, Hamdaoui M. Almond shell waste (Prunus dulcis): Functionalization with [dimethyl-diallyl-ammonium-chloride-diallylamin-co-polymer] and chitosan polymer and its investigation in dye adsorption. Journal of Molecular Liquids. 2017;240:35-44. Available from: [<URL>](#).
- 14 Mohamed HS, Soliman N, Abdelrheem DA, Ramadan AA, Elghandour AH, Ahmed SA. Adsorption of Cd²⁺ and Cr³⁺ ions from aqueous solutions by using residue of Padina gymnospora waste as promising low-cost adsorbent. Heliyon. 2019;5(3). Available from: [<URL>](#).
- 15 Rabie AM, Abukhadra MR, Rady AM, Ahmed SA, Labena A, Mohamed HS, et al. Instantaneous

- photocatalytic degradation of malachite green dye under visible light using novel green Co-ZnO/algae composites. *Research on Chemical Intermediates*. 2020;46:1955-73. Available from: [<URL>](#).
16. Naim MM, El Abd YM. Removal and recovery of dyestuffs from dyeing wastewaters. *Separation and Purification Methods*. 2002;31(1):171-228. Available from: [<URL>](#).
17. Ul-Islam S. *Advanced Materials for Wastewater Treatment*: John Wiley & Sons; 2017.
18. Kiran S, Nosheen S, Abrar S, Javed S, Aslam N, Afzal G, et al. Remediation of textile effluents via physical and chemical methods for a safe environment. *Textiles and Clothing*. 2019:191-234. Available from: [<URL>](#).
19. Rathi A, Puranik S. Treatment of wastewater pollutants from direct dyes. *American dyestuff reporter*. 1999;88(7-8):42-50.
20. Chakraborty S, De S, DasGupta S, Basu JK. Adsorption study for the removal of a basic dye: experimental and modeling. *Chemosphere*. 2005;58(8):1079-86. Available from: [<URL>](#).
21. Mohamed HS, Soliman N, Abdelrheem DA, Ramadan AA, Elghandour AH, Ahmed SA. Adsorption of Cd²⁺ and Cr³⁺ ions from aqueous solutions by using residue of *Padina gymnospora* waste as promising low-cost adsorbent. *Heliyon*. 2019;5(3):e01287. Available from: [<URL>](#).
22. Rabie AM, Abukhadra MR, Rady AM, Ahmed SA, Labena A, Mohamed HS, et al. Instantaneous photocatalytic degradation of malachite green dye under visible light using novel green Co-ZnO/algae composites. *Research on Chemical Intermediates*. 2020;46(3):1955-73. Available from: [<URL>](#).
23. Soliman N, Mohamed HS, Ahmed SA, Sayed FH, Elghandour AH, Ahmed SA. Cd²⁺ and Cu²⁺ removal by the waste of the marine brown macroalga *Hydroclathrus clathratus*. *Environmental Technology & Innovation*. 2019;15:100365. Available from: [<URL>](#).
24. Dey AK, Dey A, Goswami RJAWS. Adsorption characteristics of methyl red dye by Na₂CO₃-treated jute fibre using multi-criteria decision making approach. 2022;12(8):1-22.
25. Goswami R, Dey AKJAJoC. Synthesis and application of treated activated carbon for cationic dye removal from modelled aqueous solution. 2022;15(11):104290. Available from: [<URL>](#).
26. Dey AK, Dey AJGfSD. Selection of optimal processing condition during removal of Reactive Red 195 by NaOH treated jute fibre using adsorption. 2021;12:100522.
27. Khan MM, Dey AJMC, Physics. Hybrid MCDM approach for examining the high-stress abrasive wear behaviour of in situ ZA-27/TiCp MMCs. 2022;277:125319. Available from: [<URL>](#).
28. Bichave MS, Kature AY, Koranne SV, Shinde RS, Gongle AS, Choudhari VP, et al. Nano-metal oxides-activated carbons for dyes removal: A review. 2022. Available from: [<URL>](#).
29. Yang X, Zhu W, Song Y, Zhuang H, Tang HJJoML. Removal of cationic dye BR46 by biochar prepared from *Chrysanthemum morifolium* Ramat straw: A study on adsorption equilibrium, kinetics and isotherm. 2021;340:116617. Available from: [<URL>](#).
30. Faccenda HB, Melara F, Damini G, Godinho M, Manera C, Piccin JSJES, et al. Graywater treatment of emerging pollutant linear alkylbenzene sulfonate by adsorption with leather shave waste activated carbon. 2022;29(53):79830-40. Available from: [<URL>](#).
31. Zhang M, Li W, Jin ZJJoHM. Structural properties of deprotonated naphthenic acids immersed in water in pristine and hydroxylated carbon nanopores from molecular perspectives. 2021;415:125660. Available from: [<URL>](#).
32. Verma AK, Dash AK, Bhunia P, Dash RRJS, Interfaces. Removal of surfactants in greywater using low-cost natural adsorbents: A review. 2021;27:101532. Available from: [<URL>](#).
33. Sharaf A, Liu YJC. Mechanisms and kinetics of greywater treatment using biologically active granular activated carbon. 2021;263:128113. Available from: [<URL>](#).
34. Mohamed HS, Soliman N, Moustafa A, Abdel-Gawad OF, Taha RR, Ahmed SA. Nano metal oxide impregnated Chitosan-4-nitroacetophenone for industrial dye removal. *International Journal of Environmental Analytical Chemistry*. 2021;101(13):1850-77. Available from: [<URL>](#).
35. Mohamed HS, Tawfik WZ, Hamza ZS, Kfayf YR, El-Bassuony AA, Ahmed SA, et al. Removal of dye by adsorption on nitric acid treated sugar bagasse wastes, an experimentally, theoretically, and computational studies. *Russian Journal of Physical Chemistry A*. 2022;96(14):3232-43. Available from: [<URL>](#).
36. Ahsaine HA, Zbair M, El Haouti R. Mesoporous treated sewage sludge as outstanding low-cost adsorbent for cadmium removal. *Desalin Water Treat*. 2017;85:330-8. Available from: [<URL>](#).
37. Parra Parra A, Márquez Aguilar PA, Semjonova J, Serrano Nava ME, Vlasova M. Adsorption properties of carbonized Sargassum algae. *MRS Advances*. 2022:1-6. Available from: [<URL>](#).
38. Liranzo-Gómez RE, García-Cortés D, Jáuregui-Haza U. Adaptation and sustainable management of massive influx of Sargassum in the Caribbean. *Procedia Environ Sci Eng Manag*. 2021;8:543-53. Available from: [<URL>](#).
39. Turner A, Lewis MS, Shams L, Brown MT. Uptake of platinum group elements by the marine macroalga, *Ulva lactuca*. *Marine Chemistry*. 2007;105(3-4):271-80. Available from: [<URL>](#).
40. Jabli MJJobm. Synthesis, characterization, and assessment of cationic and anionic dye adsorption performance of functionalized silica immobilized chitosan bio-polymer. 2020;153:305-16. Available from: [<URL>](#).
41. Abd El-Hamid HT, AlProl AE, Hafiz MA. The efficiency of adsorption modelling and Plackett-Burman design for remediation of crystal violet by *Sargassum latifolium*. *Biocatalysis and Agricultural Biotechnology*. 2022;44:102459. Available from: [<URL>](#).
42. Tka N, Jabli M, Saleh TA, Salman GA. Amines modified fibers obtained from natural *Populus tremula* and

- their rapid biosorption of Acid Blue 25. *Journal of Molecular Liquids*. 2018;250:423-32. Available from: [<URL>](#).
43. khamis Soliman N, Moustafa AF, Aboud AA, Halim KSA. Effective utilization of Moringa seeds waste as a new green environmental adsorbent for removal of industrial toxic dyes. *Journal of Materials Research and Technology*. 2019;8(2):1798-808. Available from: [<URL>](#).
44. Khedr M, Halim KA, Soliman N. Synthesis and photocatalytic activity of nano-sized iron oxides. *Materials Letters*. 2009;63(6-7):598-601 Available from: [<URL>](#).
45. Lagergren SK. About the theory of so-called adsorption of soluble substances. *Sven Vetenskapsakad Handlingar*. 1898;24:1-39.
46. Kang YL, Toh SKS, Monash P, Ibrahim S, Saravanan P. Adsorption isotherm, kinetic and thermodynamic studies of activated carbon prepared from *Garcinia mangostana* shell. *Asia-Pacific Journal of Chemical Engineering*. 2013;8(6):811-8.
47. Azizian S. Kinetic models of sorption: a theoretical analysis. *Journal of colloid and Interface Science*. 2004;276(1):47-52. Available from: [<URL>](#).
48. Çoruh S, Geyikçi F, Nuri Ergun O. Adsorption of basic dye from wastewater using raw and activated red mud. *Environmental technology*. 2011;32(11):1183-93. Available from: [<URL>](#).
49. Depci T, Kul AR, Onal Y, Disli E, Alkan S, Turkmenoglu ZF. ADSORPTION OF CRYSTAL VIOLET FROM AQUEOUS SOLUTION ON ACTIVATED CARBON DERIVED FROM GÖLBAŞI LIGNITE. *Physicochemical Problems of Mineral Processing*. 2012;48(1). Available from: [<URL>](#).
50. Langmuir I. The adsorption of gases on plane surfaces of glass, mica and platinum. *Journal of the American Chemical society*. 1918;40(9):1361-403.
51. Freundlich H. Over the adsorption in solution. *J Phys Chem*. 1906;57(385471):1100-7.
52. Ozdemir O, Armagan B, Turan M, Celik MS. Comparison of the adsorption characteristics of azo-reactive dyes on mesoporous minerals. *Dyes and pigments*. 2004;62(1):49-60. Available from: [<URL>](#).
53. Demirbas E, Nas M. Batch kinetic and equilibrium studies of adsorption of Reactive Blue 21 by fly ash and sepiolite. *Desalination*. 2009;243(1-3):8-21. Available from: [<URL>](#).
54. Serna-Carrizales JC, Collins-Martínez VH, Flórez E, Gomez-Duran CF, Palestino G, Ocampo-Pérez R. Adsorption of sulfamethoxazole, sulfadiazine and sulfametazine in single and ternary systems on activated carbon. Experimental and DFT computations. *Journal of Molecular Liquids*. 2021;324:114740. Available from: [<URL>](#).
55. Abd El-Mageed H, Taha M. Exploring the intermolecular interaction of serine and threonine dipeptides with gold nanoclusters and nanoparticles of different shapes and sizes by quantum mechanics and molecular simulations. *Journal of Molecular Liquids*. 2019;296:111903. Available from: [<URL>](#).
56. Sun H, Ren P, Fried J. The COMPASS force field: parameterization and validation for phosphazenes. *Computational and Theoretical Polymer Science*. 1998;8(1-2):229-46. Available from: [<URL>](#).
57. Mohamed N, Sabaa M, El-Ghandour A, Abel-Aziz M, Abdel-Gawad O. Preparation, characterization and antimicrobial activity of carboxymethyl chitosan Schiff bases with different benzaldehyde derivatives. *Journal of American Science*. 2013;9(3):247-64.
58. Li Y-M, Sun S-Q, Zhou Q, Qin Z, Tao J-X, Wang J, et al. Identification of American ginseng from different regions using FT-IR and two-dimensional correlation IR spectroscopy. *Vibrational spectroscopy*. 2004;36(2):227-32. Available from: [<URL>](#).
59. Gliemann G. K. Nakamoto: *Infrared and Raman Spectra of Inorganic and Coordination Compounds*. John Wiley and Sons, New York, Chichester, Brisbane, Toronto 1978. 3. Aufl., XV, 448 Seiten mit 109 Abbildungen und 95 Tabellen. Preis: \$31, 15. Wiley Online Library; 1978.
60. Mishra A, Jha B. Isolation and characterization of extracellular polymeric substances from micro-algae *Dunaliella salina* under salt stress. *Bioresource technology*. 2009;100(13):3382-6. Available from: [<URL>](#).
61. Marimuthu J, Essakimuthu P, Narayanan J, Anantham B, Tharmaraj RJJM, Arumugam S. Phytochemical characterization of brown seaweed *Sargassum wightii*. *Asian Pacific Journal of Tropical Disease*. 2012;2:5109-513. Available from: [<URL>](#).
62. Diem M, Chiriboga L, Yee H. Infrared spectroscopy of human cells and tissue. VIII. Strategies for analysis of infrared tissue mapping data and applications to liver tissue. *Biopolymers: Original Research on Biomolecules*. 2000;57(5):282-90. Available from: [<URL>](#).
63. Sharma YC. Optimization of parameters for adsorption of methylene blue on a low-cost activated carbon. *Journal of Chemical & Engineering Data*. 2010;55(1):435-9. Available from: [<URL>](#).
64. Raval NP, Shah PU, Shah NK. Nanoparticles loaded biopolymer as effective adsorbent for adsorptive removal of malachite green from aqueous solution. *Water Conservation Science and Engineering*. 2016;1(1):69-81. Available from: [<URL>](#).
65. Mohan SV, Rao NC, Karthikeyan J. Adsorptive removal of direct azo dye from aqueous phase onto coal based sorbents: a kinetic and mechanistic study. *Journal of hazardous materials*. 2002;90(2):189-204. Available from: [<URL>](#).
66. Foo K, Hameed B. Preparation, characterization and evaluation of adsorptive properties of orange peel based activated carbon via microwave induced K₂CO₃ activation. *Bioresource technology*. 2012;104:679-86. Available from: [<URL>](#).
67. Ansari R, Mosayebzadeh Z. Removal of Eosin Y, an anionic dye, from aqueous solutions using conducting electroactive polymers. 2010.
68. Heibati B, Rodriguez-Couto S, Al-Ghouti MA, Asif M, Tyagi I, Agarwal S, et al. Kinetics and thermodynamics of enhanced adsorption of the dye AR 18 using activated carbons prepared from walnut and poplar woods. *Journal of Molecular Liquids*. 2015;208:99-105. Available from: [<URL>](#).
69. Elkady M, Hussein M, Salama M. Synthesis and characterization of nano-activated carbon from El Maghara Coal, Sinai, Egypt to be utilized for wastewater purification. *American Journal of Applied Chemistry*. 2015;3(3):1-7.

70. Ho Y-S, Chiu W-T, Wang C-C. Regression analysis for the sorption isotherms of basic dyes on sugarcane dust. *Bioresource technology*. 2005;96(11):1285-91. Available from: [<URL>](#).
71. Özcan AS, Erdem B, Özcan A. Adsorption of Acid Blue 193 from aqueous solutions onto BTMA-bentonite. *Colloids and Surfaces A: Physicochemical and Engineering Aspects*. 2005;266(1-3):73-81. Available from: [<URL>](#).
72. Hall KR, Eagleton LC, Acrivos A, Vermeulen T. Pore- and solid-diffusion kinetics in fixed-bed adsorption under constant-pattern conditions. *Industrial & Engineering Chemistry Fundamentals*. 1966;5(2):212-23. Available from: [<URL>](#).
73. Yadav S, Srivastava V, Banerjee S, Weng C-H, Sharma YC. Adsorption characteristics of modified sand for the removal of hexavalent chromium ions from aqueous solutions: Kinetic, thermodynamic and equilibrium studies. *Catena*. 2013;100:120-7. Available from: [<URL>](#).
74. Lin Y, He X, Han G, Tian Q, Hu W. Removal of Crystal Violet from aqueous solution using powdered mycelial biomass of *Ceriporia lacerata* P2. *Journal of Environmental Sciences*. 2011;23(12):2055-62. Available from: [<URL>](#).
75. Chen Z, Wang T, Jin X, Chen Z, Megharaj M, Naidu R. Multifunctional kaolinite-supported nanoscale zero-valent iron used for the adsorption and degradation of crystal violet in aqueous solution. *Journal of colloid and interface science*. 2013;398:59-66. Available from: [<URL>](#).
76. Sarabadan M, Bashiri H, Mousavi SM. Removal of crystal violet dye by an efficient and low cost adsorbent: modeling, kinetic, equilibrium and thermodynamic studies. *Korean Journal of Chemical Engineering*. 2019;36(10):1575-86. Available from: [<URL>](#).
77. Saeed A, Sharif M, Iqbal M. Application potential of grapefruit peel as dye sorbent: kinetics, equilibrium and mechanism of crystal violet adsorption. *Journal of hazardous materials*. 2010;179(1-3):564-72. Available from: [<URL>](#).
78. Amodu OS, Ojumu TV, Ntwampe SK, Ayanda OS. Rapid adsorption of crystal violet onto magnetic zeolite synthesized from fly ash and magnetite nanoparticles. *Journal of Encapsulation and Adsorption Sciences*. 2015;5(04):191. Available from: [<URL>](#).

